

Crystal structure and spin crossover behavior of the $[\text{Fe}(\text{5-Cl-qsal})_2][\text{Ni}(\text{dmit})_2] \cdot 2\text{CH}_3\text{CN}$ complex

Bruno J.C. Vieira, Joana T. Coutinho, João C. Dias, José C. Nunes, Isabel C. Santos, Laura C.J. Pereira, Vasco da Gama, João C. Waerenborgh*

^C²TN, CFMUL, Instituto Superior Técnico, Universidade de Lisboa, 2695-066 Bobadela LRS, Portugal

ARTICLE INFO

Article history:

Received 1 August 2014

Accepted 28 September 2014

Available online 7 October 2014

Keywords:

Spin crossover

Two-step transition

Magnetic properties

Iron

N, O ligands

ABSTRACT

The synthesis of the $[\text{Fe}(\text{5-Cl-qsal})_2][\text{Ni}(\text{dmit})_2] \cdot 2\text{CH}_3\text{CN}$ (**1**) is reported in the present work. The crystal structures of **1**, solved at 150, 245, 255 and 294 K, revealed the presence of low spin (LS) and high spin (HS) Fe^{III} centers at 150 and 294 K, respectively, and mixed HS/LS states ~50:50 and 75:25 at 245 and 255 K. The crystal structure is based on alternating cationic and anionic layers, where each layer is composed of an arrangement of chains of cations or anions. The anionic chains consist on the stacking of face-to-face pairs of $[\text{Ni}(\text{dmit})_2]^-$ anions. Extended $\pi\pi$ contacts, involving the 5-Cl-qsal ligands, were observed in the cationic chains. The contribution of the anions to the magnetization correlates well with an alternating chain, dominated by antiferromagnetic interactions. A spin crossover (SCO) process, assigned to the $[\text{Fe}(\text{5-Cl-qsal})_2]^+$ cationic network was observed at high temperatures ($T \sim 240$ K). The thermal dependence of the magnetization suggests the existence of an abrupt change at ~ 233 K from the LS state to a mixed 50:50 HS/LS state, followed by a gradual transformation at ~ 256 K to the HS state. A structural transformation consisting of the doubling of the unit cell was observed to be associated with the SCO process.

© 2014 Elsevier Ltd. All rights reserved.

1. Introduction

Research in spin crossover (SCO) compounds has been extremely active in the last years, concerning fundamental aspects of the SCO phenomenon [1], the synthesis of new materials [2], and possible technological applications [1,3]. The SCO phenomenon has been observed in metal complexes with the electronic configuration $3d^n$ ($4 \leq n \leq 7$) when the energy difference between the high spin (HS) and the low spin (LS) states is of the order of magnitude of the thermal energy (kT). The electronic ground state of these spin crossover complexes can be reversibly switched by the application of an external stimulus such as temperature, pressure, light, or magnetic field [1]. Two-step transitions occur frequently in mononuclear complexes where the metal stands on two (or more) different lattice sites, with distinct SCO transitions temperatures for each site [4]. In a few situations this process was found to be associated with a symmetry breaking in the crystal structure [5].

Multifunctionality has been one of the hot topics in materials science [1,6], since it allows the coexistence of properties in the

same material that otherwise would be very difficult to observe in traditional materials. One of the most successful approaches to multifunctional materials is the synthesis of hybrid materials build up from two molecular networks, where each network contributes different properties to the material. Materials exhibiting new properties may also be obtained, as a result of the interaction between the two networks. In this context the incorporation of SCO complexes as a building block in hybrid materials seems quite promising. New materials where the SCO phenomenon is associated with magnetic networks, liquid crystalline properties, electrical conductivity, non-linear optics, among others have been prepared [7]. Metal bis-dithiolene complexes have been used in hybrid networks incorporating SCO molecular components in order to obtain systems exhibiting magnetic [8] or conducting networks [9] coupled with a SCO transition. The preparation of switchable conductive materials, exhibiting switching near room temperature is a challenge that has been pursued mainly by the use of SCO hybrid materials, incorporating Fe^{III} complexes of Schiff base ligands, such as qsal, sal_2 -trien, and planar metal bis-dithiolenes to insure electrical conductivity. The Fe complexes often give origin to materials exhibiting SCO at temperatures not far from room temperature, displaying a strong cooperativity due to strong $\pi\pi$ interactions through the extended aromatic fragments of the ligands [10].

* Corresponding author. Tel.: +351 21 994 6220.

E-mail address: jcarlos@ctn.ist.utl.pt (J.C. Waerenborgh).

Metal bis-dithiolenes complexes have been used extensively in the synthesis of molecular conductors (and superconductors) [11]. With this goal we decided to combine the $[\text{Ni}(\text{dmit})_2]^-$ and $[\text{Fe}(5\text{-Cl-qsal})_2]^+$ and here we report the synthesis of $[\text{Fe}(5\text{-Cl-qsal})_2][\text{Ni}(\text{dmit})_2]$. The anions are expected to rap around the 5-Cl-qsal ligands of the Fe complexes, establishing $\pi\pi$ contacts that should lead to a good cooperativity in the SCO transition. Subsequent work will be focused on the preparation of salts of the partially oxidized anion, which are expected to exhibit electrical conductivity.

2. Experimental

2.1. Materials and methods

The mixing of equimolar acetonitrile solutions of $\text{TBP}[\text{Ni}(\text{dmit})_2]$ (where TBP denotes tetrabutylphosphonium) and $[\text{Fe}(5\text{-Cl-qsal})_2]\text{BF}_4$ or $[\text{Fe}(5\text{-Cl-qsal})_2]\text{BPh}_4 \cdot \text{H}_2\text{O}$ allowed the preparation of $[\text{Fe}(5\text{-Cl-qsal})_2][\text{Ni}(\text{dmit})_2] \cdot x\text{CH}_3\text{CN}$, with $x=1$, which precipitated upon cooling. Using dry acetonitrile and rigorous moisture exclusion, crystallization procedures provided $[\text{Fe}(5\text{-Cl-qsal})_2][\text{Ni}(\text{dmit})_2] \cdot 2\text{CH}_3\text{CN}$ (**1**). A detailed description of the synthesis is provided below in Section 2.2.

A summary of the crystal data, experimental details and refinement results are listed in Table 1, while selected bond distance and angle are presented in Table 2. The X-ray diffraction experiments were performed with a Bruker AXS APEX CCD detector diffractometer using graphite monochromated Mo $K\alpha$ radiation source ($\lambda = 0.71073 \text{ \AA}$), in the ψ and ω scan modes. A semi-empirical absorption correction was carried out using SADABS [12]. Data collection, cell refinement and data reduction were done with the SMART and SAINT programs [13]. The structures were solved by direct methods using SIR97 [14] and refined by full-matrix least-squares methods using the program SHELXL97 [15] using a WINGX software package [16]. Non-hydrogen atoms were refined with anisotropic thermal parameters, whereas H-atoms were placed in idealized positions and allowed to refine riding on the parent C atom. Molecular graphics were prepared using Ortep3 [17] and Mercury [18]. The CCDC reference numbers are 859397 (294 K), 875394 (255 K), 875393 (245 K), and 859398 (150 K). There is at 255 K and 245 K a doubling of the unit cell when compared to 294 K

and 150 K. As referred below this increase in unit cell volume results from the symmetry-breaking during the LS/HS transition leading to two distinct cations and anions (with non-equivalent bond lengths and angles as well as short contacts). The best structure refinement is however achieved in the same space group ($P1$) of the 294 K and 150 K phases. Slightly higher anisotropies of the atomic displacement parameters (cif files, [Supplementary material](#)) are also related to some disorder that may occur during the LS/HS transition.

Magnetic measurements were performed on a S700X SQUID magnetometer with a 7 T magnet (Cryogenic Ltd.). The temperature dependence of the magnetic susceptibility in the temperature range 2–320 K was measured under a magnetic field of 1 T. The paramagnetic susceptibility was obtained from the experimental magnetization data after a diamagnetism correction was estimated from the tabulated Pascal constants as $-665.2 \times 10^{-6} \text{ emu/mol}$. Three samples were studied. In order to check the stability of the crystals during SQUID measurements each sample was subjected to at least two heating and cooling cycles and the corresponding χT versus T curves were found to be reproducible.

Mössbauer spectra were collected in the 4–297 K temperature range, in transmission mode, using a conventional constant-acceleration spectrometer and a 25 mCi ^{57}Co source in a Rh matrix. The velocity scale was calibrated using $\alpha\text{-Fe}$ foil. Isomer shifts are given relative to metallic $\alpha\text{-Fe}$ at 297 K. A disk-shaped absorber was obtained by gently packing single crystals into a perspex holder. The absorber thickness was calculated on the basis of the electronic mass-absorption coefficient for the 14.4 keV radiation, according to Long et al. [19]. Low-temperature spectra were collected using a liquid-helium JANIS bath cryostat, model SVT-400, with the sample in He exchange gas or, for measurements at 4 K, immersed in liquid He. The spectra were fitted to Lorentzian lines using a non-linear least-squares method [20].

2.2. Synthesis

Commercial solvents were used without further purification unless otherwise specified. Reactants commercially obtained: $\text{TBP}[\text{Ni}(\text{dmit})_2]$ from TCI Europe N.V., 8-aminoquinoline, 5-chlorosalicylaldehyde, $\text{FeCl}_3 \cdot 6\text{H}_2\text{O}$ and NaBPh_4 from Aldrich. The purity of the complexes and their solvation state was verified

Table 1
Crystal data and structural refinement of compound **1**, at 150, 245, 255 and 294 K.

Temperature	150 K	245 K	255 K	294 K
Crystal size (mm)	$0.20 \times 0.18 \times 0.03$	$0.30 \times 0.16 \times 0.06$	$0.30 \times 0.16 \times 0.06$	$0.20 \times 0.16 \times 0.04$
Crystal colour and shape	black plate	black plate	black plate	black plate
Empirical formula	$\text{C}_{42}\text{H}_{26}\text{Cl}_2\text{FeNi}_6\text{NiO}_2\text{S}_{10}$	$\text{C}_{42}\text{H}_{26}\text{Cl}_2\text{FeNi}_6\text{NiO}_2\text{S}_{10}$	$\text{C}_{42}\text{H}_{26}\text{Cl}_2\text{FeNi}_6\text{NiO}_2\text{S}_{10}$	$\text{C}_{42}\text{H}_{26}\text{Cl}_2\text{FeNi}_6\text{NiO}_2\text{S}_{10}$
Molecular mass	1152.75	1152.75	1152.75	1152.75
Crystal system	triclinic	triclinic	triclinic	triclinic
Space group (No.)	$P1$	$P1$	$P1$	$P1$
a (Å)	11.6801(2)	11.8907(2)	12.3193(3)	12.0421(2)
b (Å)	12.2188(3)	18.0497(3)	18.0958(4)	12.3247(3)
c (Å)	18.0527(5)	22.9284(4)	22.2911(5)	18.0007(4)
α (°)	99.9750(10)	72.1030(10)	72.1030(10)	105.3680(10)
β (°)	102.8860(10)	83.4860(10)	83.4860(10)	98.5160(10)
γ (°)	111.7640(10)	76.0550 (10)	76.0550 (10)	112.4290(10)
V (Å ³)	2237.39(9)	4540.70(13)	4546.92(18)	2286.22(8)
Z	2	4	4	2
D_{calc} (Mg m ⁻³)	1.711	1.686	1.684	1.675
μ (mm ⁻¹)	1.378	1.358	1.358	1.349
$F(000)$	1168	2336	2336	1168
θ range (°)	3.04–25.68	2.78–25.03	2.74–25.03	3.01–25.03
Index range (h, k, l)	–14/14, –14/14, –22/22	–13/14, –21/21, –27/27	–14/13, –21/21, –26/25	–14/14, –14/14, –21/20
Reflection collected/unique (R_{int})	18884/8474 (0.0358)	64105/15989 (0.0421)	49764/15937 (0.0435)	19678/7940 (0.0383)
$T_{\text{max/min}}$	0.9598/0.7701	0.9229/0.6861	0.9229/0.6861	0.9480/0.7742
Goodness-of-fit (GOF) on F^2	0.967	0.840	0.848	1.006
Final R_1 , [$I > 2\sigma(I)$], wR_2	0.0368/0.0780	0.0305/0.0734	0.0355/0.0783	0.0398/0.0886

Table 2Selected bond lengths (Å) and angles (°) for compound **1** at 150, 245, 255 and 294 K.

	150 K	245 K		255 K		294 K
		Cation	CationA	Cation	CationA	
Fe(1)–O(1)	1.889(2)	1.888(5)	1.885(5)	1.924(5)	1.883(5)	1.981(2)
Fe(1)–O(2)	1.881(2)	1.898(5)	1.897(5)	1.887(5)	1.926(5)	1.869(2)
Fe(1)–N(1)	1.955(2)	2.052(5)	2.041(5)	2.069(6)	2.087(5)	2.074(3)
Fe(1)–N(2)	1.983(2)	2.072(6)	2.074(5)	2.087(6)	2.109(6)	2.177(3)
Fe(1)–N(3)	1.955(2)	2.030(5)	2.033(5)	2.068(5)	2.074(5)	2.116(3)
Fe(1)–N(4)	1.982(2)	2.063(5)	2.066(6)	2.102(5)	2.106(6)	2.137(3)
O(2)–Fe(1)–O(1)	91.84(9)	92.4(2)	92.2(2)	92.0(2)	92.5(2)	89.45(11)
O(2)–Fe(1)–N(1)	88.02(9)	95.2(2)	95.2(2)	97.6(2)	98.4(2)	94.31(10)
O(1)–Fe(1)–N(1)	94.62(9)	92.5(2)	91.3(2)	90.2(2)	89.8(2)	86.43(10)
O(2)–Fe(1)–N(3)	94.68(9)	92.0(2)	90.4(2)	90.4(2)	90.0(2)	95.46(10)
O(1)–Fe(1)–N(3)	88.53(9)	94.4(2)	94.9(2)	97.4(2)	97.2(2)	102.55(10)
N(1)–Fe(1)–N(3)	175.78(10)	169.8(2)	171.5(2)	168.8(2)	168.8(2)	166.78(11)
O(2)–Fe(1)–N(4)	176.90(9)	170.4(2)	170.4(2)	168.4(2)	168.4(2)	166.14(10)
O(1)–Fe(1)–N(4)	89.59(9)	90.5(2)	90.6(2)	90.5(2)	91.2(2)	95.10(10)
N(1)–Fe(1)–N(4)	94.60(10)	93.8(2)	93.9(2)	93.7(2)	92.6(2)	99.03(10)
N(3)–Fe(1)–N(4)	82.61(10)	78.7(2)	80.2(2)	78.1(2)	78.62	70.79(10)
O(2)–Fe(1)–N(2)	90.05(10)	90.3(2)	90.2(2)	913(2)	90.8(2)	92.35(11)
O(1)–Fe(1)–N(2)	176.64(9)	171.1(2)	171.0(2)	168.5(2)	167.8(2)	166.71(10)
N(1)–Fe(1)–N(2)	82.67(9)	78.9(2)	79.8(2)	78.4(2)	78.1(2)	80.31(11)
N(3)–Fe(1)–N(2)	94.08(9)	93.9(2)	93.8(2)	93.6(2)	94.4(2)	90.39(11)
N(4)–Fe(1)–N(2)	88.65(10)	88.2(2)	88.5(2)	88.5(2)	87.9(2)	86.23(10)

determining the carbon, hydrogen, nitrogen and sulfur contents at the C²TN Elemental Analysis Service.

2.2.1. [Fe(5-Cl-qsal)₂]Cl·3H₂O

A mixture of 8-aminoquinoline, 720.9 mg (5 mmol), 5-chlorosalicylaldehyde, 782.9 mg (5 mmol), and 35 mL of methanol was refluxed for 4 h. After cooling to room temperature, a solution of FeCl₃·6H₂O, 675.8 mg (2.5 mmol) and triethylamine, 506 mg (5 mmol), in 25 mL of methanol was added and the mixture was left with stirring overnight. After collection, the product was recrystallized in methanol, which after volume reduction, yielded the chloride salt, 839.7 mg (47%). Elemental *Anal.* Calc. for (Mw = 708.8): C, 54.23; H, 3.70; N, 7.90. Found: C, 54.02; H, 3.64; N, 7.85%.

2.2.2. [Fe(5-Cl-qsal)₂]BPh₄·H₂O

In air atmosphere, a solution of NaBPh₄, 68.0 mg (0.2 mmol) in 1 mL of hot methanol was added to a filtered solution of [Fe(5-Cl-qsal)₂]Cl·3H₂O, 141.8 mg (0.2 mmol), in 20 mL of hot methanol. After cooling the solution was put standing overnight, and the precipitate was then collected. The product was dried under vacuum and heating (~80 °C). 166.0 mg (87%). Elemental *Anal.* Calc. for (Mw = 956.5): C, 70.32; H, 4.43; N, 5.86. Found: C, 69.88; H, 3.57; N, 5.97%.

2.2.3. [Fe(5-Cl-qsal)₂][Ni(dmit)₂]_xCH₃CN (0 < x < 2)

In an air atmosphere, a filtered solution of TBP[Ni(dmit)₂], 71.1 mg (0.1 mmol), in 25 mL of hot acetonitrile was added slowly to a filtered solution of [Fe(5-Cl-qsal)₂]BPh₄·H₂O, 95.6 mg (0.1 mmol), in 20 mL of hot acetonitrile. The mixture was left standing overnight at 4 °C. The precipitate was collected and dried with heating overnight under vacuum. Yield: 89.0 mg (81%). Elemental *Anal.* Calc. for (Mw = 1071.0): C, 42.63; H, 1.88; N, 5.23; S, 29.95. Found: C, 43.06; H, 1.99; N, 6.22; S, 28.75%.

2.2.4. [Fe(5-Cl-qsal)₂][Ni(dmit)₂]₂·2CH₃CN (**1**)

Crystals of this compound usable for X-ray diffraction were obtained by slow evaporation of an acetonitrile solution of [Fe(5-Cl-qsal)₂][Ni(dmit)₂]₂·xCH₃CN. Acetonitrile was previously dried by refluxing with P₂O₅ (1% w/v) under N₂, followed by degassing (by freezing at 77 K under vacuum) in order to remove

residual oxygen. Crystals were collected by filtration and washed with cold diethyl ether. Elemental *Anal.* Calc. for **1** (Mw = 1152.8): C, 43.76; H, 2.27; N, 7.29; S, 27.82. Found: C, 42.63; H, 1.91; N, 7.12; S, 27.97%.

3. Results and discussion

3.1. Crystal structure of compound **1**

Compound **1** crystallizes in the triclinic space, space group *P* $\bar{1}$ both at 294(2) K and 150(2) K, where the asymmetric unit contains one cation unit, one anion unit and two solvent molecules on general positions. Fig. 1 shows the standard ORTEP with 50% thermal ellipsoids and atom numbering of both cation and anion residues at high temperature, Table 1 presents the crystallographic parameters and Table 2 selected bond lengths and angles.

The coordination bond lengths around the Fe^{III} center at 294(2) K are consistent with those reported for the [Fe(qsal)₂]⁺ in the HS state [21], suggesting that the complex is near 100% in the HS state. At this temperature the average metal–ligand distances increase in the order Fe–O (1.925 Å) < Fe–N_{imi} (2.095 Å) < Fe–N_{pyr} (2.157 Å). At 150(2) K, the average coordination distances follow the same trend with Fe–O (1.885 Å) < Fe–N_{imi} (1.955 Å) < Fe–N_{pyr} (1.983 Å). The coordination bond lengths around this center and those reported for [Fe(qsal)₂]⁺ in the low-spin (LS) state [22] are compatible, which suggest the LS state for the Fe^{III} center at 150 K.

The Fe^{III} octahedral site is distorted due to the shorter Fe–O distances compared to the Fe–N distances (see Table 2). Each 5-Cl-qsal ligand forms a substantially distorted plane: the dihedral angles between the phenyl and the quinoline rings of each ligand are 7.03(10)° and 5.05(10)° at 294(2) K (5.09(10)° and 7.19(10)° at 150(2) K), respectively, while the dihedral angles between the phenyl ring and the Fe1–O1–N1 chelate ring, the quinoline ring and the Fe1–N1–N2 chelate ring, the other phenyl ring and the Fe1–O2–N3 chelate ring, and the other quinoline ring and the Fe1–N3–N4 chelate ring are 2.87(10)°, 0.93(10)°, 1.70(10)° and 1.61(10)° at 294(2) K [2.75(10)°, 0.79(10)°, 2.68(10)°, 2.29(10)° at 150(2) K], respectively. The two tridentate ligands are almost orthogonal: the least squares planes between ligands is 88.25(10)° at 294(2) K (87.31(10)° at 150(2) K).

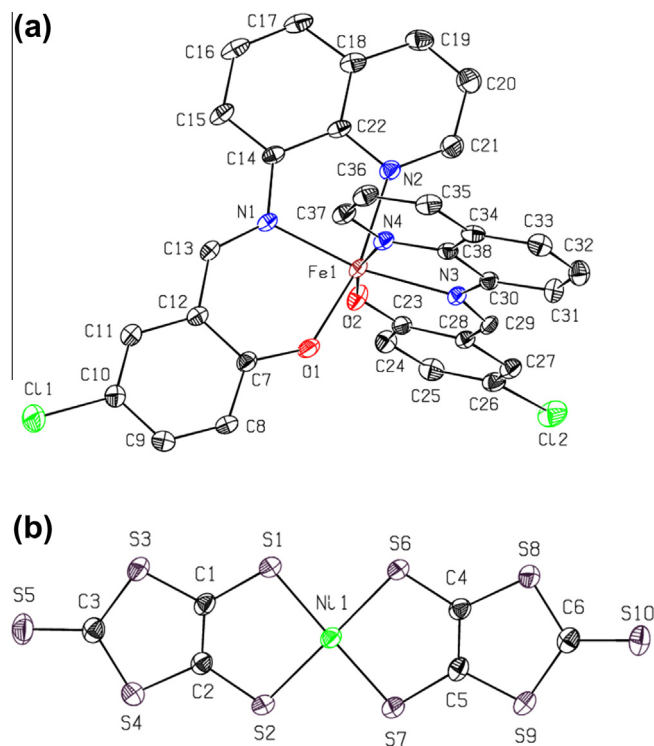


Fig. 1. ORTEP diagram with 50% thermal ellipsoids and atom numbering scheme for (a) the cationic unit and (b) the anionic unit of **1** at 294(2) K. Hydrogen atoms were omitted for clarity. (The numbering scheme for 150(2) K is the same.)

The $[\text{Ni}(\text{dmit})_2]^-$ units present a slightly distorted square planar geometry around the Ni^{III} center (see Table 2) and the complex is almost planar: the angle between the least-squares planes of the two dmit ligands is $2.83(6)^\circ$ at 294(2) K ($4.01(6)^\circ$ at 150(2) K).

The crystal structure of **1** is based on arrangements of segregated chains of the $[\text{Fe}(5\text{-Cl-qsal})_2]^+$ cations and of the $[\text{Ni}(\text{dmit})_2]^-$ anions. A view of the crystal structure of **1** along the b axis is shown in Fig. 2. Within the chains the molecular units interact strongly with the neighboring molecules, mainly through CC $\pi\pi$ interactions, in the case of the cations, and SS (or SC) contacts in the case of the anions. These chains are confined by solvent molecules, which, establishing contacts with similar molecules (cations or anions) give rise to the formation of sheets of cations and anions. Two neighboring chains plus their vicinity are shown in Fig. 3. The chains of cations present a slight modulation in the Fe–Fe distances as well as in the contacts between the π systems of the 5-Cl-qsal ligands (a cationic chain is shown in Fig. 4).

The anionic chains can be described as regular chains of face-to-face dimers of anions (AA). In these AA dimers the average distance between the average planes of the anionic molecules is 3.553 \AA , and short intradimer AA contacts are observed, involving S and C atoms of the dmit ligands. Short interdimer intrachain AA (SS) contacts are also found (an illustration of the anionic chain is shown in Fig. 5). The planarity of the cation ligands and of the anion molecules allows the existence of short interactions between the anions and cations through the overlap of the π systems of the qsal ligands and of the anions. These interactions are reinforced by extra S–C contacts between the anions and the qsal ligand that is perpendicular to the anion, as illustrated in Fig. 3. The chains of anions are isolated from each other by solvent and cation molecules.

The cationic chains are relatively isolated and present only short contacts involving the Cl atoms from the ligands at high temperatures ($d = 3.406 \text{ \AA}$). At low temperatures, with the structural

distortion associated with the SCO transition these contacts vanish ($d = 4.362 \text{ \AA}$) and Cl–C contacts ($d = 3.409 \text{ \AA}$) appear at low temperatures. However a large number of indirect connections between the cationic chains are present (mediated by the solvent or anionic molecules) and could lead to the existence of a good overall connectivity between the SCO centers. Besides the change in the inter-chain contacts, mentioned above, a slight variation in the superposition mode of the anions with the dimers is detected as illustrated in Fig. 6 representing a top view of the face-to-face anions (at 300 K and at 150 K). It is possible to observe that the slippage between the two molecules is larger at low temperatures. No other significant variations in the supramolecular arrangements associated with the SCO process are detected (selected intermolecular contacts are summarized in Table S1 in Supporting information).

The peculiar magnetic behavior detected in the SCO process (see below) lead us to examine the possible occurrence of a two-step SCO process, similar to that observed in a variety of $\text{Fe}^{\text{II/III}}$ compounds [4,5]. In order to investigate the variation of the crystal structure in the vicinity of the SCO transition ($\sim 220\text{--}260 \text{ K}$) we acquired further data in this temperature range and we detected a doubling of the unit cell above the transition. The structure was solved at 245 and 255 K (crystal data and structural refinement of compound **1** at 245 and 255 K are shown in Table 1). Data collected at higher temperatures ($T > 260 \text{ K}$) could not be fitted to a doubled unit cell.

The crystal structures obtained at 245 and 255 K include two crystallographically distinct cations and anions, but unlike the case of the systems displaying two-step SCO with an ordered intermediate phase [4,5], in compound **1** the coordination distances for both Fe^{III} atoms are similar in both cations. At 245 K, the average coordination distances, Fe–O, Fe– N_{imi} , Fe– N_{pyr} , are 1.893, 2.041 and 2.068 \AA , for one cation and 1.891, 2.037 and 2.070 \AA for the other, and these values lie midway between those obtained at 150 K (LS) and at 294 K (HS). At 255 K the average coordination distances are slightly higher, (1.906, 2.069 and 2.095 \AA and 1.905, 2.081 and 2.108) and closer to those observed at 294 K. The supramolecular arrangements are very similar to those already presented for the crystal structures obtained at 150 and 294 K. The main contacts are summarized in Table S2 (Supporting information) and the molecular arrangements, as well as the contacts in the cationic chains of the structures obtained at 150, 245, 250 and 294 K, can be seen in Fig. S1 in Supporting information. The minor changes of the anionic sublattice and rearrangement in the solvent molecules detected during the progress of the SCO process are illustrated in Fig. S2 in Supporting information.

The transition from the LS phase to the disordered intermediate phase with 50:50 LS/HS at 236 K, seems to induce a significant stress in the crystal structure and lead to a sudden increase of the volume of the structure and lowering of the lattice symmetry. With increasing temperature the crystal structure seems to gradually recover the low-temperature symmetry as the LS/HS transformation progresses. Fig. S3 (in Supporting information) shows the evolution of the cell volume with temperature.

3.2. Magnetic properties

Fig. 7 shows the temperature dependence of χT , where χ is the molar paramagnetic susceptibility of **1**. The magnetic behavior of this compound is the result of the contributions of the $[\text{Fe}(5\text{-Cl-qsal})_2]^+$ cations (with $S_{\text{C}} = 1/2$ or $5/2$) and of the $[\text{Ni}(\text{dmit})_2]^-$ anions (with a $S_{\text{A}} = 1/2$). The magnetic susceptibility is $\chi = \chi_{\text{C}} + \chi_{\text{A}}$

where χ_{C} and χ_{A} are the contributions from the cations and the anions, respectively. At low temperatures ($T < 200 \text{ K}$) the magnetic

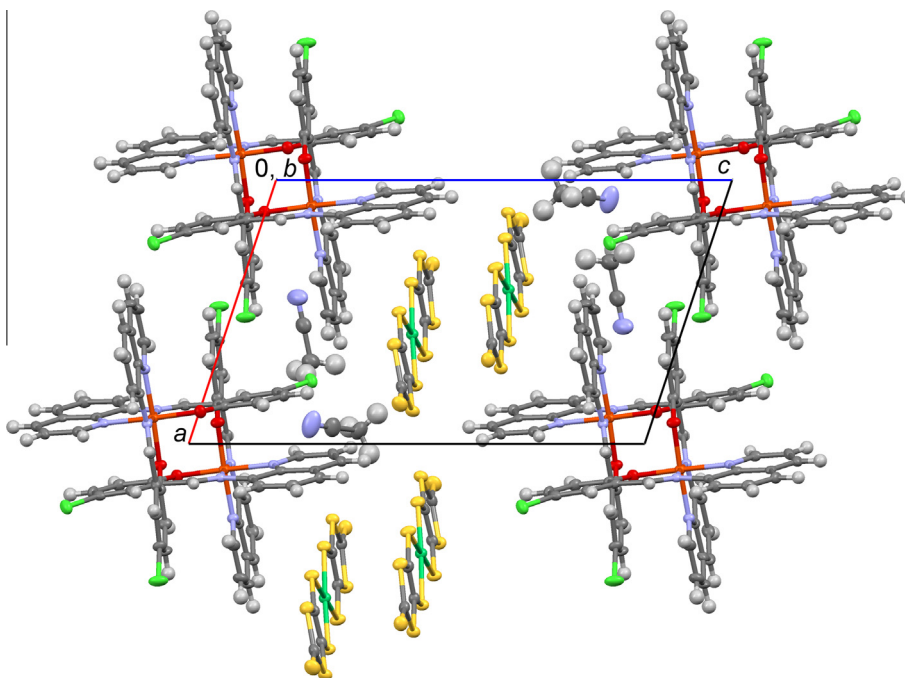


Fig. 2. View of the structure of **1** along the *b* axis.

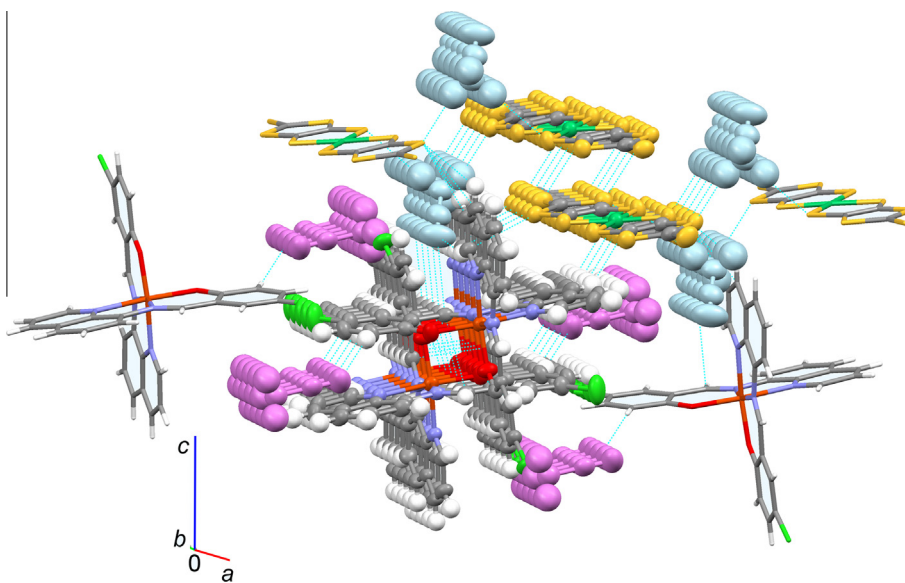


Fig. 3. Detail of the columnar arrangement, showing the cationic and anionic chains of **1** and the respective vicinity. Two distinct acetonitrile molecules confine the cationic and anionic chains.

susceptibility can be ascribed to the $S = 1/2$ cations and anions while above 200 K, the clear increase of χT , observed in **1**, indicates a SCO process.

The analysis of the crystal structure of compound **1** suggests the existence of strong magnetic interactions between the anions. In fact the delocalization of the unpaired electrons along the anion molecules, and the chain of face-to-face dimers with a large number of SS short contacts are expected to lead to strong anion–anion magnetic interactions. On the other hand the magnetic interactions involving the cations are expected to be rather weak, as most of the spin density on the cations must be located at the Fe atoms and the contacts in the periphery of the ligand are not expected to lead to significant magnetic interactions which will be neglected. The

anion–cation magnetic interactions are also expected to be rather weak and will also be ignored. In this sense the cation contribution can be described as [23]:

$$\chi_C = f\chi^{HS} + (1 - f)\chi^{LS} \quad (2)$$

where f and $1 - f$ are the high spin and low spin fractions of the Fe atoms, respectively, and χ^{HS} and χ^{LS} (the limit values of χ_C for $f = 1$ and 0) are given by the Curie Law:

$$\chi^{is} = \frac{N_A \mu_B^2}{3kt} g_{is}^2 S_{is}(S_{is} + 1) \quad (3)$$

where N_A is the Avogadro's number, μ_B is the Bohr magneton, and k is the Boltzmann constant. In view of the alternating chain

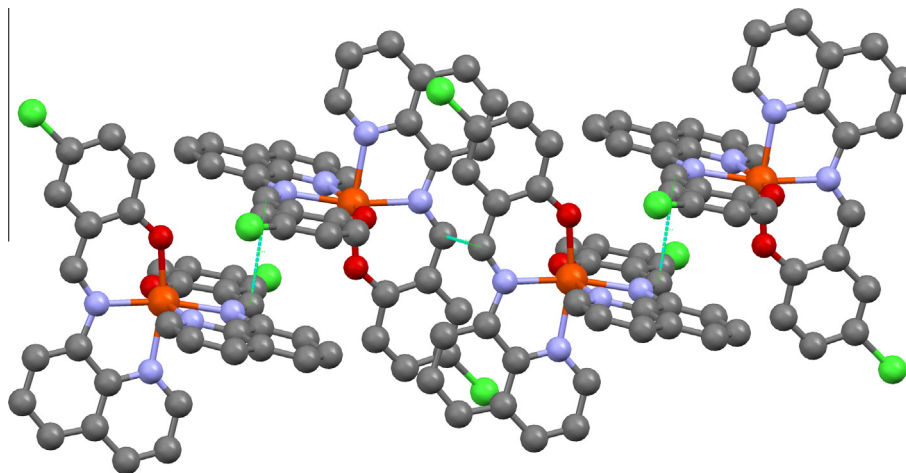


Fig. 4. Illustration of the arrangement (and intermolecular contacts) of the $[\text{Fe}(5\text{-Cl-qsal})_2]^+$ cations in the cationic chains of **1**.

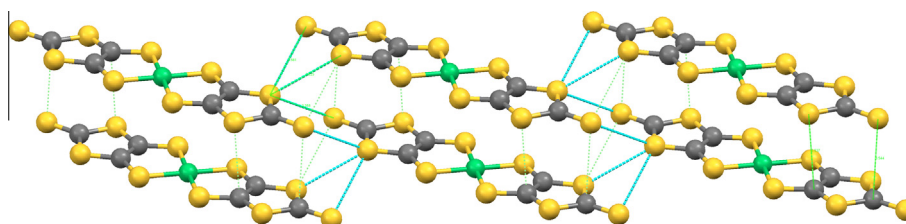


Fig. 5. Illustration of the anionic chain of **1** showing the shorter intrachain contacts. Thicker dotted lines correspond to contacts shorter than the sum of the van der Waals radii (d_W), while the thinner dotted lines to contacts slightly larger than d_W .

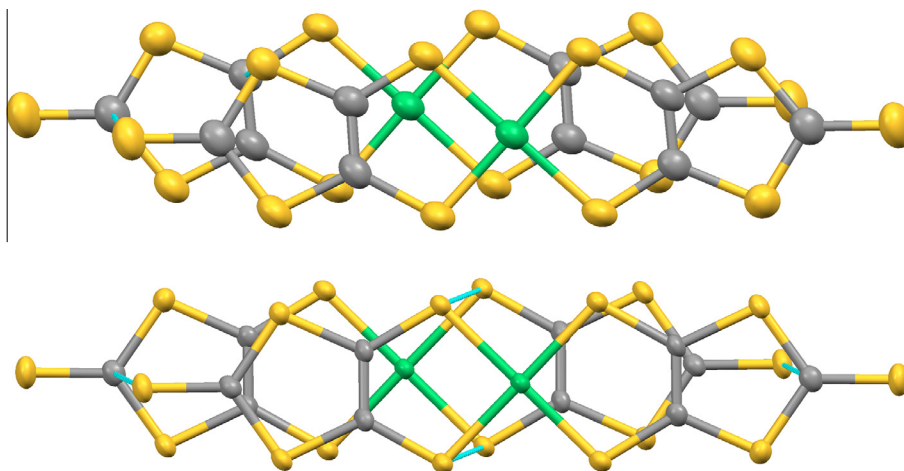


Fig. 6. View of the molecular overlap in the anionic dimers in **1** at 294 and 150 K (top and bottom).

arrangement of the anions, the contribution of the anions to χ can be described in terms of two interaction parameters, J and αJ , by the analytical expression [24]:

$$\chi_A = \frac{N_A g_A \mu_B^2}{kT} \frac{A + B\epsilon + C\epsilon^2}{1 + D\epsilon + E\epsilon^2 + F\epsilon^3} \quad \text{with } \epsilon = |J|/kT \quad (4)$$

for $0 \leq \alpha \leq 0.4$, the A–F coefficients are $A = 0.25$; $B = -0.062935 + 0.11376\alpha$; $C = 0.0047778 - 0.033268\alpha + 0.12742\alpha^2 - 0.32918\alpha^3 + 0.25203\alpha^4$; $D = 0.05386 + 0.709\alpha$; $E = -0.00071302 - 0.10587\alpha + 0.54883\alpha^2 - 0.20603\alpha^3$; $F = 0.047193 - 0.0083778\alpha + 0.87256\alpha^2 - 2.7098\alpha^3 + 1.9798\alpha^4$. Eqs. (1)–(4) were used to describe the behavior of **1** below 150 K (with $f = 0$, $S_C = S_A = 1/2$). The results obtained, $g_C = 2.25$, $g_A = 2.06$, $\alpha = 0.29$, $J = -582$ K and $\theta = -1.68$ K,

are consistent with the existence of strong antiferromagnetic (AF) intradimer coupling between the anions (associated to the interactions between the face-to-face anions), and weaker AF interdimer coupling. As expected the magnetic interaction between cations seems to be very weak. The results of the fit obtained for $T < 150$ K are represented by the dashed line in Fig. 7. The strong AF anion-anion coupling is responsible for a very small contribution from the anions (solid line).

The AA overlap within the dimers (Fig. 6) and the short AA contacts between the anions are consistent with the observed strong AF coupling observed in **1** [25]. For an intradimer ferromagnetic (FM) coupling a larger slipping of the molecules in the dimer would be required [25,26].

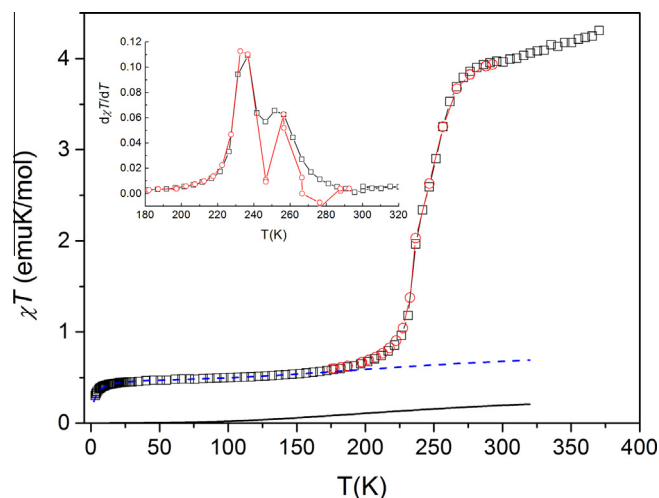


Fig. 7. Thermal variation of the χT product for compound **1**. Squares represent the measurements obtained on heating, while circles the measurements on cooling. The dashed line represents the low temperature fitting (Eqs. (1)–(4)), and the solid line the calculated contribution of the anionic network in **1**. The inset shows the thermal dependence of $d\chi T/dT$.

The SCO process observed for compound **1** is nearly completed at the highest temperatures achieved, with $\chi T = 4.31 \text{ emu K mol}^{-1}$ at 370 K. $\chi T = 4.31 \text{ emu K mol}^{-1}$ is slightly below the calculated for the HS Fe^{III} configuration with the estimated contribution from the anions, $4.57 \text{ emu K mol}^{-1}$ (with $g_c = 2$ [27] and $S_c = 5/2$). χT decreases with cooling. At high temperatures the decrease is slow, but it becomes faster at $\sim 280 \text{ K}$, decreasing regularly until 236 K , where it drops suddenly. Below 226 K χT slowly stabilizes to the expected value for LS Fe^{III} (apart the small contribution from the anions). The temperature dependence of $d\chi T/dT$ is shown in the inset of Fig. 7 (both on warming and cooling modes, represented by the squares and the circles respectively). The χT value before the sharp decrease at 236 K , $\sim \chi T = 2.34 \text{ emu K mol}^{-1}$ is close to the expected for **1** with 50% HS Fe^{III} ($2.56 \text{ emu K mol}^{-1}$), which might suggest the existence of a two-step SCO process with an HS–LS intermediate ordered state similar to that observed in a variety of compounds [21]. However the crystal structure studies clearly rule out the existence of an intermediate ordered state, and this peculiar behavior of the thermal dependence of the SCO process must be associated to structural constraints to the lattice deformation. The sharpness of the χT decrease at $\sim 236 \text{ K}$ reveals the existence of a considerable cooperativity between the SCO centers which can be assigned to the large number of $\pi\pi$ contacts between aromatic rings of the 5-Cl-qsal ligands. No noticeable hysteresis could be observed in the SCO process of **1**. Other compounds with strong $\pi\pi$ contacts show sharp SCO transitions and no hysteresis [5e,9a,28]. Although as far as we know it is not yet possible to predict when hysteresis will occur it is frequently observed when the SCO transition concurs with structural alterations extending well beyond the Fe coordination sphere.

The acetonitrile solvent molecules have an effect in the SCO transition. However it was never possible to obtain a pure desolvated compound as it always decomposed before all the solvent molecules were removed. Attempts to prepare $[\text{Fe}(\text{5-Cl-qsal})_2][\text{Ni}(\text{dmit})_2] \cdot x\text{CH}_3\text{CN}$ with $x < 2$ either gave rise to a mixture of compounds with different x or to decomposition products. No crystals suitable for X-ray diffraction were obtained either. Magnetic susceptibility measurements of the $[\text{Fe}(\text{5-Cl-qsal})_2][\text{Ni}(\text{dmit})_2] \cdot x\text{CH}_3\text{CN}$ mixtures showed a gradual transition clearly different from the sharp $[\text{Fe}(\text{5-Cl-qsal})_2][\text{Ni}(\text{dmit})_2] \cdot 2\text{CH}_3\text{CN}$ transition (Fig. S4). Results were not reproducible most likely because

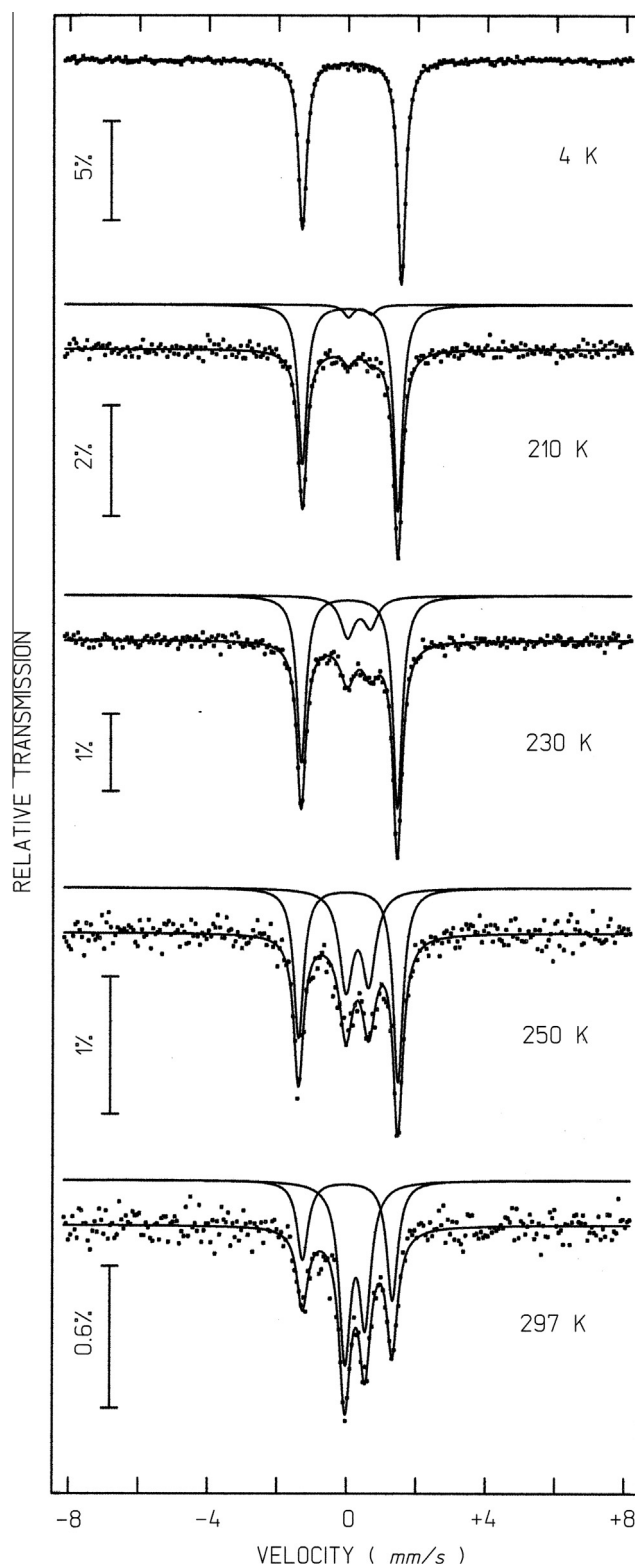


Fig. 8. Mössbauer spectra of **1** taken at different temperatures.

different mixtures did not have the same proportions of compounds with different x .

The Mössbauer spectra obtained below 200 K for **1** consist of single quadrupole doublets (Fig. 8). The relative areas of both peaks in each doublet are not equal very likely due to texture effects. These effects are expected since crystals used to prepare the

Table 3

Estimated parameters from Mössbauer spectra of compound **1** at different temperatures.

T (K)	Fe ^{III} spin	IS	QS	W	I (%)
297	LS	0.14	2.60	0.37	36
	HS	0.37	0.58	0.45	64
250	LS	0.14	2.75	0.34	57
	HS	0.40	0.66	0.47	43
230	LS	0.15	2.84	0.32	78
	HS	0.43	0.67	0.48	22
210	LS	0.16	2.86	0.31	94
	HS	0.44	0.67	0.35	6
180 4.2	LS	0.18	2.84	0.27	100
	LS	0.21	2.86	0.29	100

IS (mm/s) isomer shift relative to metallic α -Fe at 297 K; QS (mm/s) quadrupole splitting; W (mm/s) line-width; I relative area. Estimated errors: ≤ 0.02 mm/s for IS, QS, W, $< 2\%$ for I.

Mössbauer absorber have a particular cleavage that should give rise to preferred orientation effects after packing.

All the remaining spectra clearly show four absorption peaks that may be fitted with two quadrupole doublets. The estimated parameters (Table 3) for the doublet with lower splitting are typical of HS Fe^{III}. The larger quadrupole splitting, QS, and lower isomer shift, IS, estimated for the remaining doublet in each spectrum are expected for LS Fe^{III}. A fair agreement was observed between the relative quantities of HS and LS Fe^{III} in **1**, obtained by the Mössbauer spectra and the magnetic susceptibility. At higher temperatures ($T > 250$ K), the LS Fe^{III} fraction deduced from the Mössbauer spectra seems to be overestimated. This may be attributed to the different temperature dependences of the Lamb–Mössbauer factors of the HS and the LS Fe^{III} species.

4. Conclusions

The synthesis and crystallization procedures in acetonitrile solutions allowed the preparation of the SCO compound [Fe(5-Cl-qsal)₂][Ni(dmit)₂] \cdot 2CH₃CN. This compound shows a layered structure, with alternating layers based on arrangements of chains of cations and anions. Extended $\pi\pi$ contacts involving the 5-Cl-qsal ligands were observed in the cationic chains. The magnetic behavior is the sum of the contributions from the cations and anions. The anions are organized as an arrangement of dimers presenting strong intradimer AF coupling and weaker coupling between the dimers. The SCO process was characterized by magnetization measurements and Mössbauer spectroscopy. The magnetization measurements indicate that as the temperature increases the SCO occurs in two steps, one at ~ 233 K, relatively sharp, passing from a LS state to a state with 50:50 disordered HS/LS, followed by a more gradual increase of the HS content (centered at ~ 256 K) towards a HS state. The peculiar progress of the SCO process of this compound may be related to structural constraints that prevent the full LS/HS transformation in a narrow temperature range and lead to the appearance of a disordered intermediate phase with a doubled unit cell.

Acknowledgments

This work was partially supported by “Fundação para a Ciência e Tecnologia” (Portugal) under contract PTDC/QUI/65379/2006 and grants SFRH/BD/65237/2009 and SFRH/BD/84628/2012.

Appendix A. Supplementary data

CCDC 859397, 875394, 875393 and 859398 contain the supplementary crystallographic data for compound **1** at 294 K, 255 K,

245 K and 150 K, respectively. These data can be obtained free of charge via <http://www.ccdc.cam.ac.uk/conts/retrieving.html>, or from the Cambridge Crystallographic Data Centre, 12 Union Road, Cambridge CB2 1EZ, UK; fax: (+44) 1223-336-033; or e-mail: deposit@ccdc.cam.ac.uk. Supplementary data associated with this article can be found, in the online version, at <http://dx.doi.org/10.1016/j.poly.2014.09.038>.

References

- [1] P. Gütlich, H.A. Goodwin, L. Goux-Capes, in: P. Gütlich, H.A. Goodwin (Eds.), *Spin Crossover in Transition Metal Compounds I*, Top. Curr. Chem., 233, Springer-Verlag, Berlin, Heidelberg, 2004, p. 1.
- [2] T. Forestier, S. Mornet, N. Daro, T. Nishihara, S.-I. Mouri, K. Tanaka, O. Fouché, E. Freysz, J.-F. Létard, Chem. Commun. (2008) 4327.
- [3] J.-F. Létard, P. Guionneau, L. Goux-Capes, in: P. Gütlich, H.A. Goodwin (Eds.), *Spin Crossover in Transition Metal Compounds III*, Top. Curr. Chem., 235, Springer-Verlag, Berlin, Heidelberg, 2004, p. 221.
- [4] (a) Y. Garcia, O. Kahn, L. Rabardel, B. Chansou, L. Salmon, J.P. Tuchagues, Inorg. Chem. 38 (1999) 4663; (b) G.S. Matouzenko, J.-F. Létard, S. Lecocq, A. Bousseksou, L. Capes, L. Salmon, M. Perrin, O. Kahn, A. Collet, Eur. J. Inorg. Chem. (2001) 2935; (c) W. Hibbs, P.J. van Koningsbruggen, A.M. Arif, W.W. Shum, J.S. Miller, Inorg. Chem. 42 (2003) 5645; (d) P. Poganiuch, S. Decurtins, P. Gütlich, J. Am. Chem. Soc. 112 (1990) 3270; (e) R. Hinek, H. Spiering, D. Schollmeyer, P. Gütlich, A. Hauser, Chem. Eur. J. 2 (1996) 1427; (f) B. Weber, C. Carbonera, C. Desplanches, J.-F. Létard, Eur. J. Inorg. Chem. (2008) 1589; (g) B. Li, R.-J. Wei, J. Tao, R.-B. Huang, L.-S. Zheng, Z. Zheng, J. Am. Chem. Soc. 132 (2010) 1558; (h) J. Klingele, D. Kaase, M.H. Klingele, J. Lach, S. Demeshko, Dalton Trans. 39 (2010) 1689; (i) M.S. Shongwe, B.A. Al-Rashdi, H. Adams, M.J. Morris, M. Mikuriya, G.R. Hearne, Inorg. Chem. 46 (2007) 9558; (j) R.-J. Wei, B. Li, J. Tao, R.-B. Huang, L.-S. Zheng, Z. Zheng, Inorg. Chem. 50 (2011) 1170.
- [5] (a) D. Chernyshov, M. Hostettler, K.W. Tornroos, H.-B. Burgi, Angew. Chem., Int. Ed. 42 (2003) 3825; (b) S. Bonnet, M.A. Siegler, J.S. Costa, G. Molnar, A. Bousseksou, A.L. Spek, P. Gameza, J. Reedijk, Chem. Commun. (2008) 5619; (c) N. Bréfuel, H. Watanabe, L. Toupet, J. Come, N. Matsumoto, E. Collet, K. Tanaka, J.-P. Tuchagues, Angew. Chem., Int. Ed. 48 (2009) 9304; (d) M. Griffin, S. Shakespeare, H.J. Shepherd, C.J. Harding, J.-F. Létard, C. Desplanches, A.E. Goeta, J.A.K. Howard, A.K. Powell, V. Mereacre, Y. Garcia, A.D. Naik, H. Muller-Bunz, G.G. Morgan, Angew. Chem., Int. Ed. 52 (2013) 3845; (e) B.J.C. Vieira, J.T. Coutinho, I.C. Santos, L.C.J. Pereira, J.C. Waerenborgh, Vasco da Gama, Inorg. Chem. 52 (2013) 3845.
- [6] J.A. Real, A.B. Gaspar, M.C. Munoz, Dalton Trans. (2005) 2062.
- [7] For a general overview see A.B. Gaspar, V. Ksenofontov, M. Seredyuk, P. Gütlich, Coord. Chem. Rev. 249 (2005) 2661–2676.
- [8] A.I.S. Neves, J.C. Dias, B.J.C. Vieira, I.C. Santos, M.B.C. Branco, L.C.J. Pereira, J.C. Waerenborgh, M. Almeida, D. Belo, V. Gama, CrystEngComm 11 (2009) 2160.
- [9] (a) K. Takahashi, H.-B. Cui, Y. Okano, H. Kobayashi, H. Mori, H. Tajima, Y. Einaga, O. Sato, J. Am. Chem. Soc. 130 (2008) 6688; (b) C. Faulmann, K. Jacob, S. Dorbes, S. Lampert, I. Malfant, M.-L. Doublet, L. Valade, J.A. Real, Inorg. Chem. 46 (2007) 8548; (c) K. Takahashi, H.-B. Cui, Y. Okano, H. Kobayashi, Y. Einaga, O. Sato, Inorg. Chem. 45 (2006) 5739.
- [10] (a) B.R. Muller, G. Leibeling, E.-G. Jager, Chem. Phys. Lett. 319 (2000) 368; (b) O. Sato, Acc. Chem. Res. 36 (2003) 692; (c) B. Weber, E. Kaps, J. Weigand, C. Carbonera, J.-F. Létard, K. Achterhold, F.G. Parak, Inorg. Chem. 47 (2008) 487; (d) S. Dorbes, L. Valade, J.A. Real, C. Faulmann, Chem. Commun. (2005) 69.
- [11] L. Valade, C. Faulmann, in: M. Formigué, L. Ouahab (Eds.), *Conducting and Magnetic Organometallic Molecular Materials*, Topics in Organometallic Chemistry, 27, Springer-Verlag, Berlin, Heidelberg, 2009, p. 141.
- [12] G.M. Sheldrick, SHELXL97, Bruker AXS Inc., Madison, Wisconsin, USA, 2004.
- [13] Bruker, SMART and SAINT, Bruker AXS Inc., Madison, Wisconsin, USA, 2004.
- [14] A. Altomare, M.C. Burla, M. Camalli, G. Cascarano, G. Giacovazzo, A. Guagliardi, A.G.G. Moliterni, G. Polidori, R. Spagna, J. Appl. Crystallogr. 32 (1999) 115.
- [15] G.M. Sheldrick, SHELXL97, Program for Crystal Structure Refinement, University of Göttingen, Germany, 1997.
- [16] L.J. Farrugia, J. Appl. Crystallogr. 32 (1999) 837.
- [17] L.J. Farrugia, J. Appl. Crystallogr. 30 (1997) 565.
- [18] C.F. Macrae, I.J. Bruno, J.A. Chisholm, P.R. Edgington, P. McCabe, E. Pidcock, L. Rodriguez-Monge, R. Taylor, J. van de Streek, P.A. Wood, J. Appl. Crystallogr. 41 (2008) 466.
- [19] G.J. Long, T.E. Cranshaw, G. Longworth, Mossb. Effect Ref. Data J. 6 (1983) 42.
- [20] J.C. Waerenborgh, P. Salamakha, O. Sologub, A.P. Gonçalves, C. Cardoso, S. Sérgio, M. Godinho, M. Almeida, Chem. Mater. 12 (2000) 1743.
- [21] J.C. Dias, A. Soriano-Portillo, M. Clemente-Léon, C. Giménez-Saiz, J.R. Galán-Mascarós, C.J. Gómez-García, E. Coronado, Inorg. Chim. Acta 360 (2007) 3843.

- [22] S. Hayami, Z.-Z. Gu, H. Yoshiki, A. Fujishima, O. Sato, *J. Am. Chem. Soc.* 123 (2001) 11644.
- [23] R. Boča, in: *Theoretical Foundations of Molecular Magnetism, Current Methods in Inorganic Chemistry*, 1, Elsevier Amsterdam, 1999, p. 541.
- [24] O. Kahn, *Molecular Magnetism*, VCH Publishers Inc., New York, 1993. p. 251.
- [25] V. Gama, M. Almeida, *Conducting and Magnetic Organometallic Molecular Materials*, in: M. Formigué, L. Ouahab (Eds.), *Topics in Organometallic Chemistry*, 27, Springer-Verlag, Berlin, Heidelberg, 2009, p. 97.
- [26] C. Faulmann, E. Rivière, S. Dorbes, F. Senocq, E. Coronado, P. Cassoux, *Eur. J. Inorg. Chem.* (2003) 2880.
- [27] R. Boča, Y. Fukuda, M. Gembicky, R. Herchel, R. Jarosciak, W. Linert, F. Renz, J. Yuzurihara, *Chem. Phys. Lett.* 325 (2000) 411.
- [28] (a) I. Salitros, N.T. Madhu, R. Boca, J. Pavlik, M. Ruben, *Monatsh. Chem.* 140 (2009) 695;
(b) P. Koningsbruggen, Y. Maeda, H. Oshio, *Spin Crossover in Transition Metal Compounds I*, in: P. Gülich, H.A. Goodwin (Eds.), 233, Springer-Verlag, Berlin, Heidelberg, 2004, p. 259.